

# Quantile Fourier Transform, Quantile Series, and Nonparametric Estimation of Quantile Spectra\*

Ta-Hsin Li<sup>†</sup>

December 10, 2024

## Abstract

A nonparametric method is proposed for estimating the quantile spectra and cross-spectra introduced in Li (2012; 2014) as bivariate functions of frequency and quantile level. The method is based on the quantile discrete Fourier transform (QDFT) defined by trigonometric quantile regression and the quantile series (QSER) defined by the inverse Fourier transform of the QDFT. A nonparametric spectral estimator is constructed from the autocovariance function of the QSER using the lag-window (LW) approach. Smoothing techniques are also employed to reduce the statistical variability of the LW estimator across quantiles when the underlying spectrum varies smoothly with respect to the quantile level. The performance of the proposed estimation method is evaluated through a simulation study.

*Keywords:* Fourier transform, quantile-frequency analysis, quantile regression, smoothing spline, spectrum, time series.

---

\*This is an update to the earlier version in arXiv dated November 9, 2022.

<sup>†</sup>Formerly affiliated with IBM T. J. Watson Research Center. Email: THL024@OUTLOOK.COM

# 1 Introduction

The concept of quantile spectra and cross-spectra was introduced in Li (2012; 2014) through the quantile periodograms and cross-periodograms constructed from trigonometric quantile regression. Let  $\{y_{j,t}\}$  ( $j = 1, \dots, m$ ) be stationary time series with marginal distribution functions  $F_j(y) := \Pr\{y_{j,t} \leq y\}$  and density functions  $\dot{F}_j(y) > 0$  ( $j = 1, \dots, m$ ). Let  $F_{jj',\tau}(y, y') := \Pr\{y_{j,t} \leq y, y_{j',t-\tau} \leq y'\}$  ( $j, j' = 1, \dots, m$ ) be the lag- $\tau$  bivariate distribution functions and  $\phi_{jj',\tau}(y, y') := \Pr\{(y_{j,t} - y)(y_{j',t-\tau} - y') < 0\}$  ( $j, j' = 1, \dots, m$ ) be the lag- $\tau$  bivariate level-crossing rates ( $\tau = 0, \pm 1, \dots$ ). Then, the quantile spectra and cross-spectra of these series at a quantile level  $\alpha \in (0, 1)$  can be written as

$$S_{jj'}(\omega, \alpha) := \eta_j(\alpha) \eta_{j'}(\alpha) \sum_{\tau=-\infty}^{\infty} r_{jj'}(\tau, \alpha) \exp(-i\omega\tau) \quad (0 \leq \omega < 2\pi), \quad (1)$$

where

$$\begin{aligned} r_{jj'}(\tau, \alpha) &:= 1 - \frac{1}{2\alpha(1-\alpha)} \phi_{jj',\tau}(F_j^{-1}(\alpha), F_{j'}^{-1}(\alpha)) \\ &= \frac{1}{\alpha(1-\alpha)} \left\{ F_{jj',\tau}(F_j^{-1}(\alpha), F_{j'}^{-1}(\alpha)) - \alpha^2 \right\}, \\ \eta_j(\alpha) &:= \sqrt{\alpha(1-\alpha)} \kappa_j(\alpha), \end{aligned}$$

and  $\kappa_j(\alpha) := 1/\dot{F}_j(F_j^{-1}(\alpha))$ . The quantile spectra and cross-spectra are analogous to the ordinary power spectra and cross-spectra in the sense that  $\eta_j(\alpha)$  takes place of the standard deviation and  $r_{jj'}(\tau, \alpha)$  takes place of the ordinary autocorrelation function (Brockwell and Davis 1992, p. 435). Because  $r_{jj'}(\tau, \alpha)$  coincides with the ordinary autocorrelation function of the indicator processes  $\{\mathcal{I}(y_{j,t} \leq F_j^{-1}(\alpha))\}$  ( $j = 1, \dots, m$ ), the quantile spectra and cross-spectra in (1) are closely related to the spectral analysis methods for indicator processes (Davis and Mikosch 2009; Hagemann 2013; Dette et al. 2015; Baruník and Kley 2019).

While the spectra of indicator processes are typically treated as functions of  $\omega$  for fixed  $\alpha$ , we regard  $S(\omega, \alpha)$  in (1) as a bivariate function of  $\omega$  and  $\alpha$  on  $[0, 2\pi) \times (0, 1)$ . Exploration of

the quantile spectra and cross-spectra as bivariate functions constitutes what we call quantile-frequency analysis or QFA (Li 2020).

Estimating the quantile spectra and cross-spectra defined by (1) is not as straightforward as estimating the ordinary spectra and cross-spectra of indicator processes, because they are derived indirectly from the quantile periodograms and cross-periodograms. In this paper, we propose an estimation method that takes advantage of the concept of quantile discrete Fourier transform (QDFT) introduced in Li (2014).

The gist of the proposed method is as follows: First, we use the solutions of trigonometric quantile regression to construct the QDFT for each observed series  $\{y_{j,t} : t = 1, \dots, n\}$  ( $j = 1, \dots, m$ ) on a finite grid of quantile levels; then, for each quantile level, we compute the inverse Fourier transform of the QDFT to produce  $m$  sequences in the time domain, which we call quantile series (QSER); and finally, we use the sample autocovariance function of the QSER, which we call quantile autocovariance function (QACF), to construct a nonparametric estimator of the quantile spectra and cross-spectra in (1) by following the conventional lag-window (LW) approach. We further employ a smoothing procedure across quantiles when the underlying spectrum is suitably smooth with respect to the quantile level. The resulting estimator, called lag-window estimator with quantile smoothing, or LWQS, is aimed at leveraging the smoothness of the underlying spectrum to reduce the statistical variability of the LW estimator.

The remainder of this paper is organized as follows. In Section 2, we introduce the QDFT, QSER, and QACF. In Section 3, we describe the LW and LWQS estimators. In Section 4, we present the results of a simulation study on the performance of the proposed method. Concluding remarks are given in Section 5. In addition, a summary of R functions for the proposed method is provided in Appendix I, and additional results of the simulation study in Appendix II.

## 2 Quantile Fourier Transform and Quantile Series

Given a data record  $\{y_{j,t} : t = 1, \dots, n\}$  of length  $n$ , let  $\omega_v := 2\pi v/n$  ( $v = 0, 1, \dots, n-1$ ) be the  $n$  Fourier frequencies. For each  $\omega_v \notin \{0, \pi\}$ , consider the following trigonometric quantile regression solution at quantile level  $\alpha \in (0, 1)$ :

$$\begin{aligned} & \{\hat{\beta}_{1,j}(\omega_v, \alpha), \hat{\beta}_{2,j}(\omega_v, \alpha), \hat{\beta}_{3,j}(\omega_v, \alpha)\} \\ &:= \underset{\beta_1, \beta_2, \beta_3 \in \mathbb{R}}{\operatorname{argmin}} \sum_{t=1}^n \rho_\alpha(y_{j,t} - \beta_1 - \beta_2 \cos(\omega_v t) - \beta_3 \sin(\omega_v t)), \end{aligned} \quad (2)$$

where  $\rho_\alpha(y) := y(\alpha - \mathcal{I}(y \leq 0))$  is the objective function of quantile regression (Koenker 2005, p. 5). In addition, for  $\omega_v = \pi$  (i.e.,  $v = n/2$  when  $n$  is even), let

$$\begin{aligned} \{\hat{\beta}_{1,j}(\pi, \alpha), \hat{\beta}_{2,j}(\pi, \alpha)\} &:= \underset{\beta_1, \beta_2 \in \mathbb{R}}{\operatorname{argmin}} \sum_{t=1}^n \rho_\alpha(y_{j,t} - \beta_1 - \beta_2 \cos(\pi t)), \\ \hat{\beta}_{3,j}(\pi, \alpha) &:= 0, \end{aligned} \quad (3)$$

and for  $\omega_v = 0$  (i.e.,  $v = 0$ ), let

$$\begin{aligned} \hat{\beta}_{1,j}(0, \alpha) &:= \underset{\beta_1 \in \mathbb{R}}{\operatorname{argmin}} \sum_{t=1}^n \rho_\alpha(y_{j,t} - \beta_1), \\ \hat{\beta}_{2,j}(0, \alpha) &:= \hat{\beta}_{3,j}(0, \alpha) := 0. \end{aligned} \quad (4)$$

Based on these trigonometric quantile regression solutions, we define the quantile discrete Fourier transform (QDFT) of  $\{y_{j,t} : t = 1, \dots, n\}$  at quantile level  $\alpha$  as

$$Z_j(\omega_v, \alpha) := \begin{cases} n\hat{\beta}_{1,j}(0, \alpha) & v = 0, \\ n\hat{\beta}_{2,j}(\pi, \alpha) & v = n/2 \text{ (if } n \text{ is even)}, \\ (n/2)\{\hat{\beta}_{2,j}(\omega_v, \alpha) - i\hat{\beta}_{3,j}(\omega_v, \alpha)\} & \text{otherwise.} \end{cases} \quad (5)$$

This definition of QDFT is motivated by the fact that the ordinary DFT can be constructed in the same way by replacing  $\rho_\alpha(y)$  with the objective function  $y^2$  of least-squares regression.

It is easy to see that the sequence  $\{Z_j(\omega_v, \alpha) : v = 0, 1, \dots, n-1\}$  is conjugate symmetric:

$$Z_j(\omega_v, \alpha) = Z_j^*(\omega_{n-v}, \alpha) \quad (v = 1, \dots, \lfloor (n-1)/2 \rfloor). \quad (6)$$

Therefore, in order to compute the QDFT, one only need to solve the quantile regression problems (2)–(3) for  $\omega_v \in (0, \pi]$ , i.e., for  $v = 1, \dots, (n-1)/2$  when  $n$  is odd and  $v = 1, \dots, n/2$  when  $n$  is even; the conjugate symmetry property provides the values of QDFT for the remaining frequencies. Linear programming algorithms such as those implemented by the function `rq` in the R package ‘quantreg’ (Koenker 2005) can be employed to compute the quantile regression solutions efficiently.

Based on the QDFT in (5), the quantile periodogram and cross-periodogram (Li 2012; 2014) of the  $m$  series  $\{y_{j,t} : t = 1, \dots, n\}$  ( $j = 1, \dots, m$ ) at quantile level  $\alpha$  can be written as

$$Q_{jj'}(\omega_v, \alpha) := n^{-1} Z_j(\omega_v, \alpha) Z_{j'}^*(\omega_v, \alpha) \quad (v = 0, 1, \dots, n-1). \quad (7)$$

This expression of the quantile periodograms (QPER) in terms of the QDFT is consistent with the conventional definition of the ordinary periodograms in terms of the ordinary DFT (Brockwell and Davis 1992, p. 443). Under suitable conditions Li (2012; 2014, p. 557), it can be shown that  $Q_{jj'}(\omega, \alpha) \xrightarrow{D} \zeta_j \zeta_{j'}^*$  for fixed  $\omega \in (0, \pi)$  and  $\alpha \in (0, 1)$ , where  $\zeta := [\zeta_1, \dots, \zeta_m]^T$  is complex Gaussian with mean vector  $\mathbf{0}$  and covariance matrix  $\mathbf{S}(\omega, \alpha) := [S_{jj'}(\omega, \alpha)]_{j,j'=1}^m$ . This is analogous to the result for the ordinary periodogram where  $\mathbf{S}(\omega, \alpha)$  is replaced by the ordinary spectrum (Brockwell and Davis 1992, p. 446).

For each  $j = 1, \dots, m$ , we can also compute the inverse Fourier transform of the QDFT  $\{Z_j(\omega_v, \alpha) : v = 0, 1, \dots, n-1\}$ , i.e.,

$$x_{j,t}(\alpha) := \frac{1}{n} \sum_{j=0}^{n-1} Z_j(\omega_v, \alpha) \exp(it\omega_v) \quad (t = 1, \dots, n). \quad (8)$$

We call this sequence the quantile series (QSER) of  $\{y_{j,t} : t = 1, \dots, n\}$  at quantile level  $\alpha$ . Note that the QSER is a real-valued time series due to (6). Also note that the sample mean of the QSER,  $\bar{x}_j(\alpha) := n^{-1} \sum_{t=1}^n x_{j,t}(\alpha)$ , coincides with  $\hat{\beta}_{1,j}(0, \alpha)$ , which is nothing but the  $\alpha$ -quantile of  $\{y_{j,t} : t = 1, \dots, n\}$ , because  $Z_j(0, \alpha) = n \hat{\beta}_{1,j}(0, \alpha)$  by definition.

In matrix notation, let  $\mathbf{x}_t(\alpha) := [x_{1,t}(\alpha), \dots, x_{m,t}(\alpha)]^T$ . Then, the sample autocovariance function (ACF) of the QSER in (8) is given by

$$\hat{\mathbf{\Gamma}}(\tau, \alpha) := \frac{1}{n} \sum_{t=\tau+1}^n (\mathbf{x}_t(\alpha) - \bar{\mathbf{x}}(\alpha)) (\mathbf{x}_{t-\tau}(\alpha) - \bar{\mathbf{x}}(\alpha))^T \quad (\tau = 0, 1, \dots, n-1), \quad (9)$$

where  $\bar{\mathbf{x}}(\alpha) := n^{-1} \sum_{t=1}^n \mathbf{x}_t(\alpha) = [\bar{x}_1(\alpha), \dots, \bar{x}_m(\alpha)]^T$ . We call  $\hat{\mathbf{\Gamma}}(\tau, \alpha)$  in (9) the sample quantile autocovariance function (QACF) at level  $\alpha$ . It is easy to show that the usual relationship between the ordinary ACF and the ordinary periodogram (Brockwell and Davis 1992, p. 443) holds true for the QACF and the QPER, i.e.,

$$\mathbf{Q}(\omega_v, \alpha) = \sum_{|\tau| < n} \hat{\mathbf{\Gamma}}(\tau, \alpha) \exp(-i\omega_v \tau) \quad (v = 0, 1, \dots, n-1), \quad (10)$$

where  $\mathbf{Q}(\omega_v, \alpha) := [Q_{j,j'}(\omega_v, \alpha)]_{j,j'=1}^m$  and  $\hat{\mathbf{\Gamma}}(-\tau, \alpha) := \hat{\mathbf{\Gamma}}(\tau, \alpha)^T$  ( $\tau = 1, \dots, n-1$ ).

### 3 Lag-Window Spectral Estimator

Consider what we call the quantile-crossing process

$$u_{j,t}(\alpha) := \alpha - \mathcal{I}(y_{j,t} \leq F_j^{-1}(\alpha)), \quad (11)$$

which is stationary with mean 0 and variance  $\alpha(1-\alpha)$ . Under suitable conditions (Wu 2007; Li 2012), the quantile regression coefficients in (2)–(4) have the Bahadur-type representations

$$\begin{aligned} \hat{\beta}_{1,j}(0, \alpha) &= F_j^{-1}(\alpha) + \kappa_j(\alpha) n^{-1} \sum_{t=1}^n u_{j,t}(\alpha) + o_P(n^{-1/2}), \\ \hat{\beta}_{2,j}(\pi, \alpha) &= \kappa_j(\alpha) n^{-1} \sum_{t=1}^n u_{j,t}(\alpha) \cos(\pi t) + o_P(n^{-1/2}), \\ \hat{\beta}_{2,j}(\omega_v, \alpha) &= 2\kappa_j(\alpha) n^{-1} \sum_{t=1}^n u_{j,t}(\alpha) \cos(\omega_v t) + o_P(n^{-1/2}) \quad \omega_v \notin \{0, \pi\}, \\ \hat{\beta}_{3,j}(\omega_v, \alpha) &= 2\kappa_j(\alpha) n^{-1} \sum_{t=1}^n u_{j,t}(\alpha) \sin(\omega_v t) + o_P(n^{-1/2}) \quad \omega_v \notin \{0, \pi\}. \end{aligned}$$

Define

$$y_{j,t}(\alpha) := F_j^{-1}(\alpha) + \kappa_j(\alpha) u_{j,t}(\alpha).$$

It follows from the Bahadur-type representations that

$$x_{j,t}(\alpha) = y_{j,t}(\alpha) + e_{j,t}(\alpha)$$

and  $n^{-1} \sum_{t=1}^n \{e_{j,t}(\alpha)\}^2 = o_P(1)$ . Therefore,  $\hat{\Gamma}(\tau, \alpha)$  in (9) can be regarded as an estimate of the ordinary ACF of the stationary process  $\mathbf{y}_t(\alpha) := [y_{1,t}(\alpha), \dots, y_{m,t}(\alpha)]^T$ , denoted as  $\Gamma(\tau, \alpha) := [\gamma_{jj'}(\tau, \alpha)]_{j,j'=1}^m := \text{Cov}\{\mathbf{y}_t(\alpha), \mathbf{y}_{t-\tau}(\alpha)\}$ . Observe that

$$\gamma_{jj'}(\tau, \alpha) = \eta_j(\alpha) \eta_{j'}(\alpha) r_{jj'}(\tau, \alpha).$$

When  $\{\gamma_{jj'}(\tau, \alpha) : \tau = 0, \pm 1, \dots\}$  is absolutely summable for all  $j$  and  $j'$ , we have

$$\mathbf{S}(\omega, \alpha) = \sum_{\tau=-\infty}^{\infty} \Gamma(\omega, \alpha) \exp(-i\omega\tau) \quad \omega \in [0, 2\pi).$$

In light of this relationship, we take the conventional lag-window (LW) approach (Priestley 1981, p. 433) and propose the following estimator for the quantile spectrum  $\mathbf{S}(\omega, \alpha)$ :

$$\hat{\mathbf{S}}_{\text{LW}}(\omega, \alpha) := \sum_{|\tau| < n} h(\tau/M) \hat{\Gamma}(\tau, \alpha) \exp(-i\omega\tau), \quad (12)$$

where  $\hat{\Gamma}(\tau, \alpha)$  is the QACF given by (9) and  $h(x)$  is a suitable nonnegative function, an example of which is the Tukey-Hanning window (Priestley 1981, p. 443)

$$h(x) := \frac{1}{2}(1 + \cos(\pi x)) \mathcal{I}(|x| \leq 1). \quad (13)$$

In the spectral case where  $h(x) = 1$  and  $M = n - 1$ , the LW estimator  $\hat{\mathbf{S}}_{\text{LW}}(\omega_v, \alpha)$  becomes the quantile periodogram  $\mathbf{Q}(\omega_v, \alpha)$  ( $v = 0, 1, \dots, n - 1$ ) according to (10).

The LW estimator is expected to work well estimating  $\mathbf{S}(\omega, \alpha)$  as a function of  $\omega$  for fixed  $\alpha$ . There are situations where  $\mathbf{S}(\omega, \alpha)$  is smooth in  $\alpha$  as well. For example,  $S(\omega, \alpha)$  is continuous in  $\alpha$  when (a)  $\dot{F}_j(F_j^{-1}(\alpha))$  is continuous in  $\alpha$  for all  $j$ , (b)  $r_{jj'}(\tau, \alpha)$  is continuous in  $\alpha$  for all  $j$ ,  $j'$ , and  $\tau$ , and (c)  $r_{jj'}(\tau, \alpha)$  is uniformly summable over  $\tau$  for all  $j$  and  $j'$ . In such cases, further improvement in estimation accuracy is expected if the smoothness is properly taken into account.

This can be accomplished, for example, by first evaluating the LW estimator on a finite grid of quantile levels  $\{\alpha_\ell : \ell = 1, \dots, L\}$  and then applying a smoothing procedure to the resulting sequence  $\{\hat{S}_{\text{LW}}(\omega, \alpha_\ell) : \ell = 1, \dots, L\}$  for fixed  $\omega$ . We will refer to the LW estimator with post-smoothing across quantiles as the LWQS estimator.

## 4 Simulation Study

To investigate the performance of the estimation method outlined in the previous section, we use a set of simulated data with  $m = 2$  and  $n = 512$ . The first series,  $\{y_{1,t}\}$ , is a nonlinear mixture of these components  $\{\xi_{1,t}\}$ ,  $\{\xi_{2,t}\}$ , and  $\{\xi_{3,t}\}$ :

$$\begin{cases} z_t &:= \psi_1(\xi_{1,t}) \times \xi_{1,t} + (1 - \psi_1(\xi_{1,t})) \times \xi_{2,t}, \\ y_{1,t} &:= \psi_2(z_t) \times z_t + (1 - \psi_2(z_t)) \times \xi_{3,t}, \end{cases} \quad (14)$$

where  $\psi_1(u) := 0.9\mathcal{I}(u < -0.8) + 0.2\mathcal{I}(u > 0.8) + \{0.9 - (7/16)(u + 0.8)\}\mathcal{I}(|u| \leq 0.8)$  and  $\psi_2(u) := 0.5\mathcal{I}(u < -0.4) + \mathcal{I}(u > 0.4) + \{0.5 + (5/8)(u + 0.4)\}\mathcal{I}(|u| \leq 0.4)$ . The second series,  $\{y_{2,t}\}$ , is a delayed copy of  $\{\xi_{3,t}\}$ :

$$y_{2,t} := \xi_{3,t-10}. \quad (15)$$

The three components are zero-mean unit-variance autoregressive (AR) processes, satisfying

$$\begin{aligned} \xi_{1,t} &= a_{11} \xi_{1,t-1} + \varepsilon_{1,t}, \\ \xi_{2,t} &= a_{21} \xi_{2,t-1} + \varepsilon_{2,t}, \\ \xi_{3,t} &= a_{31} \xi_{3,t-1} + a_{32} \xi_{3,t-2} + \varepsilon_{3,t}, \end{aligned}$$

where  $a_{11} := 0.8$ ,  $a_{21} := -0.7$ ,  $a_{31} := 2r\cos(2\pi f_0)$  and  $a_{32} := -r^2$  with  $r = 0.9$ ,  $f_0 = 0.2$ , and where  $\{\varepsilon_{1,t}\}$ ,  $\{\varepsilon_{2,t}\}$ , and  $\{\varepsilon_{3,t}\}$  are mutually independent Gaussian white noise. In other words,  $\{\xi_{1,t}\}$  is a low-pass series with spectral peak at frequency 0,  $\{\xi_{2,t}\}$  is a high-pass series with

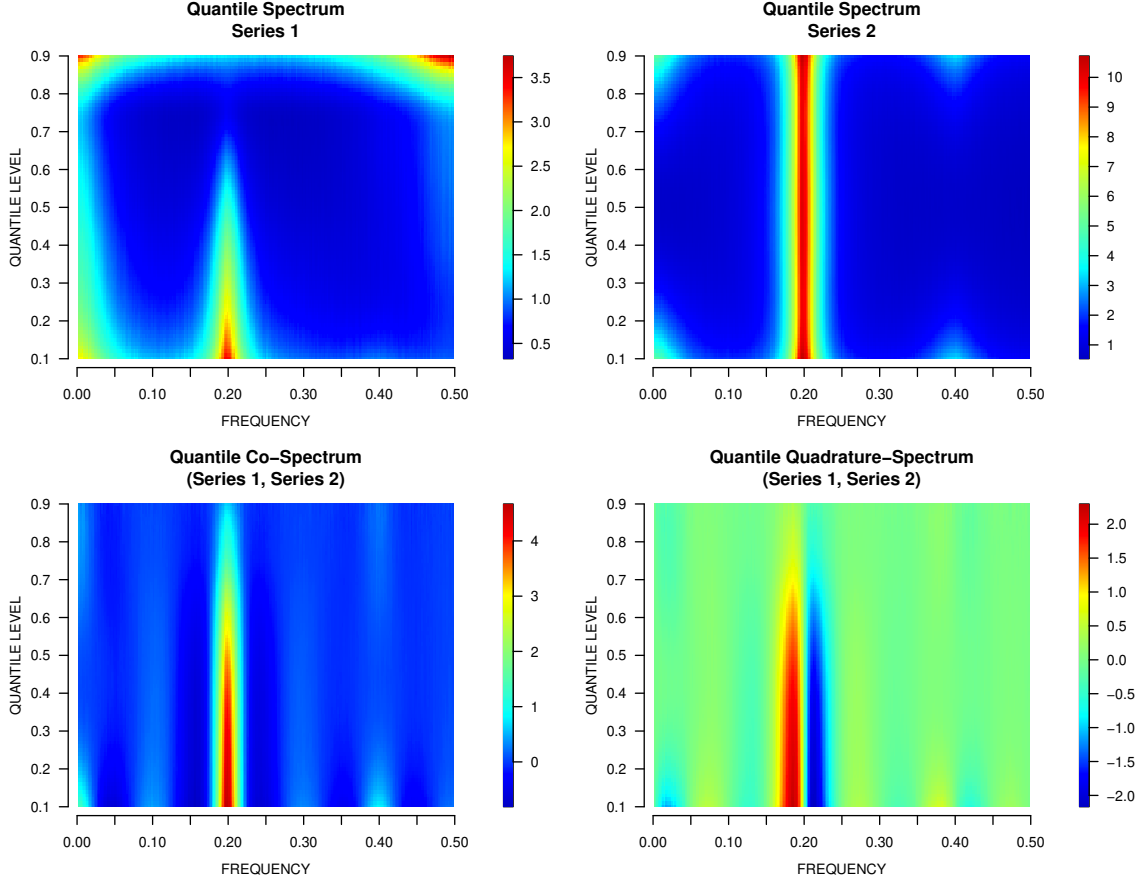


Figure 1: Quantile spectrum and cross-spectrum for the time series given by (14) and (15). All spectra are shown as functions of linear frequency  $f := \omega/(2\pi) \in (0, 0.5)$ .

spectral peak at frequency  $\pi$ , and  $\{\xi_{3,t}\}$  is a band-pass series with spectral peak at frequency  $0.2 \times 2\pi$ . The mixing function  $\psi_1(u)$  and  $\psi_2(u)$  are designed to promote or reduce these spectral patterns at different quantile regions.

Figure 1 shows the quantile spectrum and cross-spectrum of the series in (14)-(15) evaluated at  $\omega_v = 2\pi v/512$  ( $v = 1, \dots, 255$ ) and  $\alpha_\ell = 0.1 + 0.01(\ell - 1)$  ( $\ell = 1, \dots, 81$ ). These spectra are computed as the ensemble mean of quantile periodograms and cross-periodograms from 5000 Monte Carlo runs. The cross-spectrum is shown by its real and complex parts in the second row of Figure 1, which are known as co-spectrum and quadrature-spectrum, respectively,

Figure 2 shows the series from one of the simulation runs. The corresponding quantile pe-

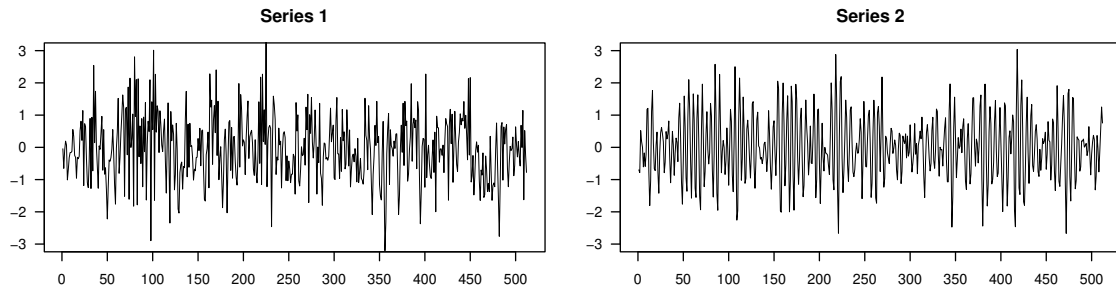


Figure 2: An example of simulated time series ( $n = 512$ ) according to (14) and (15).

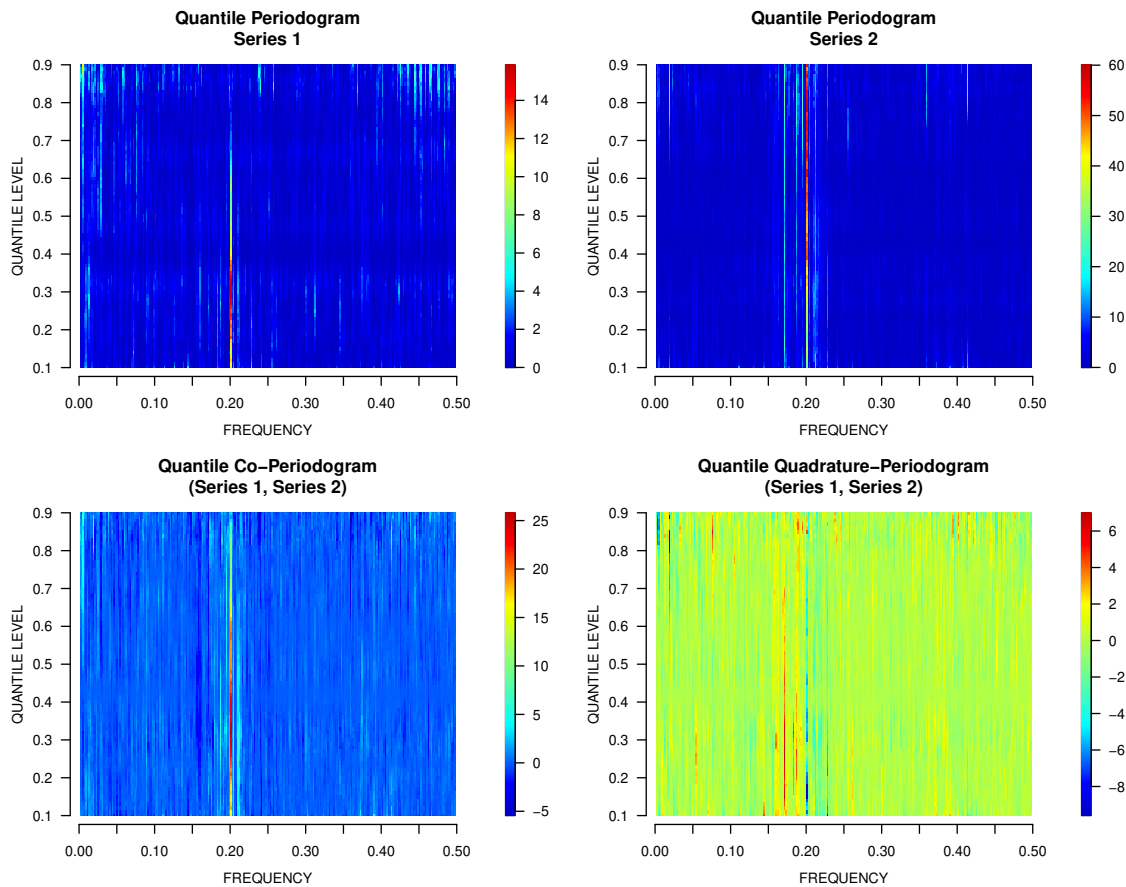


Figure 3: Quantile periodogram and cross-periodogram for the series shown in Figure 2.

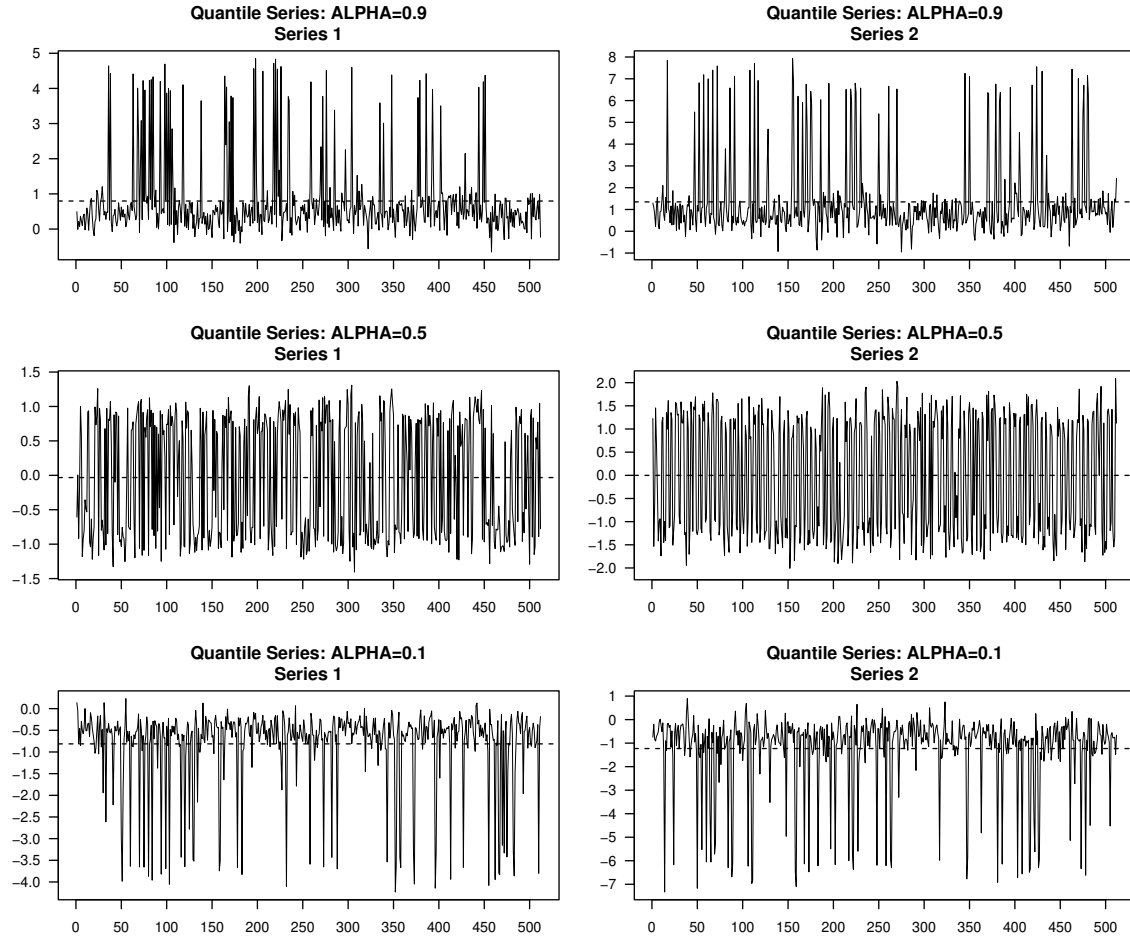


Figure 4: Time-series plot of quantile series for the series shown in Figure 2 at  $\alpha = 0.9$  (first row),  $\alpha = 0.5$  (second row), and  $\alpha = 0.1$  (third row). Dashed horizontal line depicts the sample mean of the quantile series.

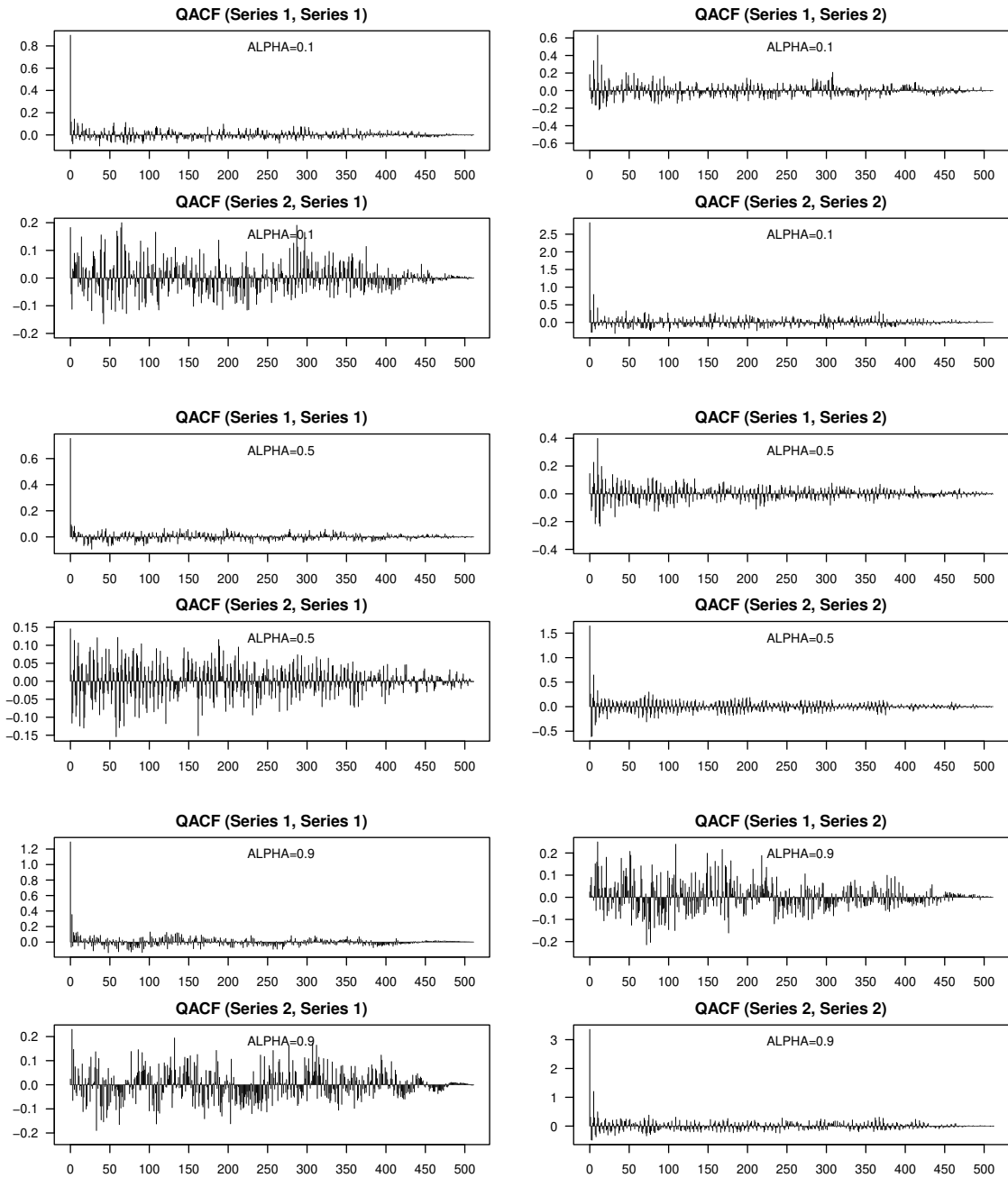


Figure 5: QACF of the series shown in Figure 2 at  $\alpha = 0.1, 0.5$ , and  $0.9$ .

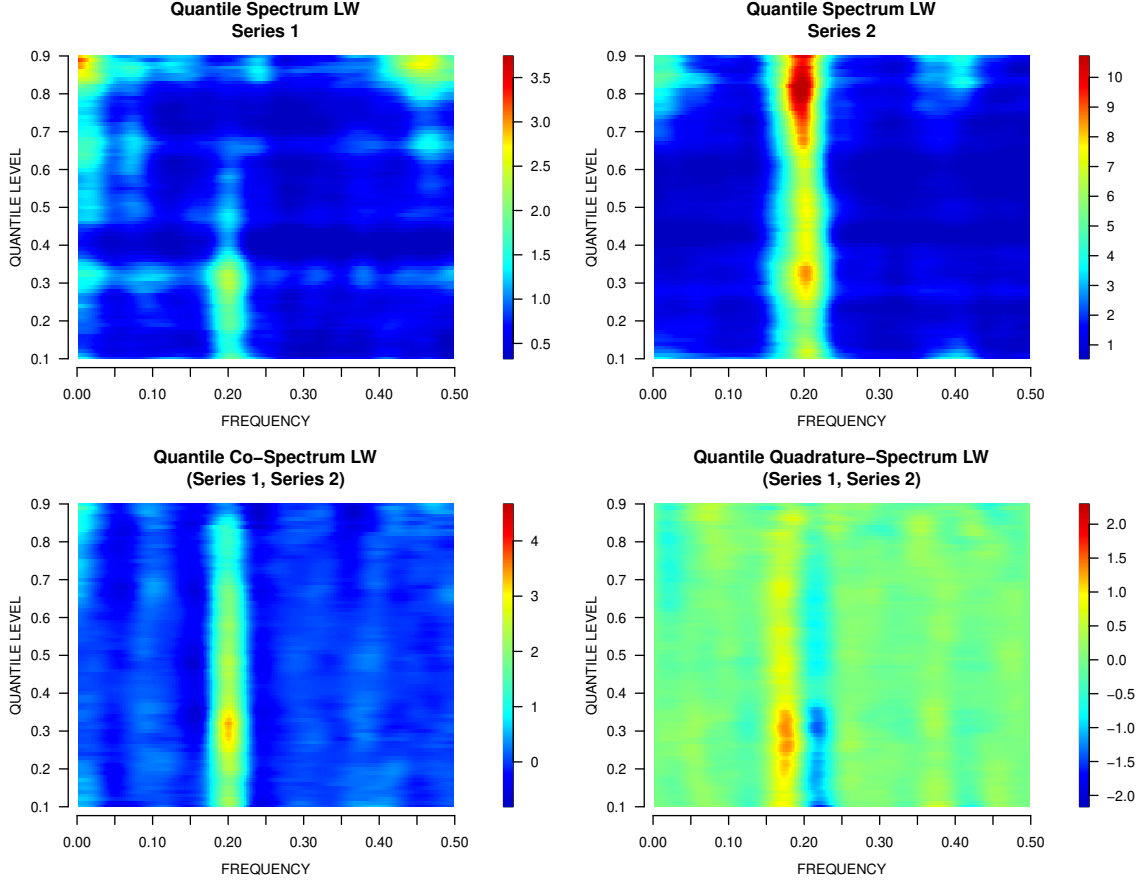


Figure 6: LW estimates of the quantile spectrum and cross-spectrum shown in Figure 1 from the series shown in Figure 2.  $KLD = 0.198$ .

riodogram and cross-periodogram are shown in Figure 3. Figure 4 depicts the QSER of these series at  $\alpha = 0.1, 0.5$ , and  $0.9$ . The corresponding QACFs are shown in Figure 5.

Figure 6 shows the LW spectral estimates obtained from the series in Figure 2. These estimates are constructed according to (12) using the Tukey-Hanning window (13) with  $M = 30$ . They can be viewed as a smoothed version of the raw quantile periodogram and cross-periodogram in Figure 3 with respect to the frequency variable.

To measure the accuracy of spectral estimation, we employ the Kullback-Leibler divergence

$$KLD := \frac{1}{L \lfloor (n-1)/2 \rfloor} \sum_{\ell=1}^L \sum_{v=1}^{\lfloor (n-1)/2 \rfloor} \left\{ \text{tr}(\hat{\mathbf{S}}(\omega_v, \alpha_\ell) \mathbf{S}^{-1}(\omega_v, \alpha_\ell)) - \log \frac{|\hat{\mathbf{S}}(\omega_v, \alpha_\ell)|}{|\mathbf{S}(\omega_v, \alpha_\ell)|} - m \right\}.$$

This spectral measure is closely related to Whittle's likelihood (Whittle 1953) and has been used

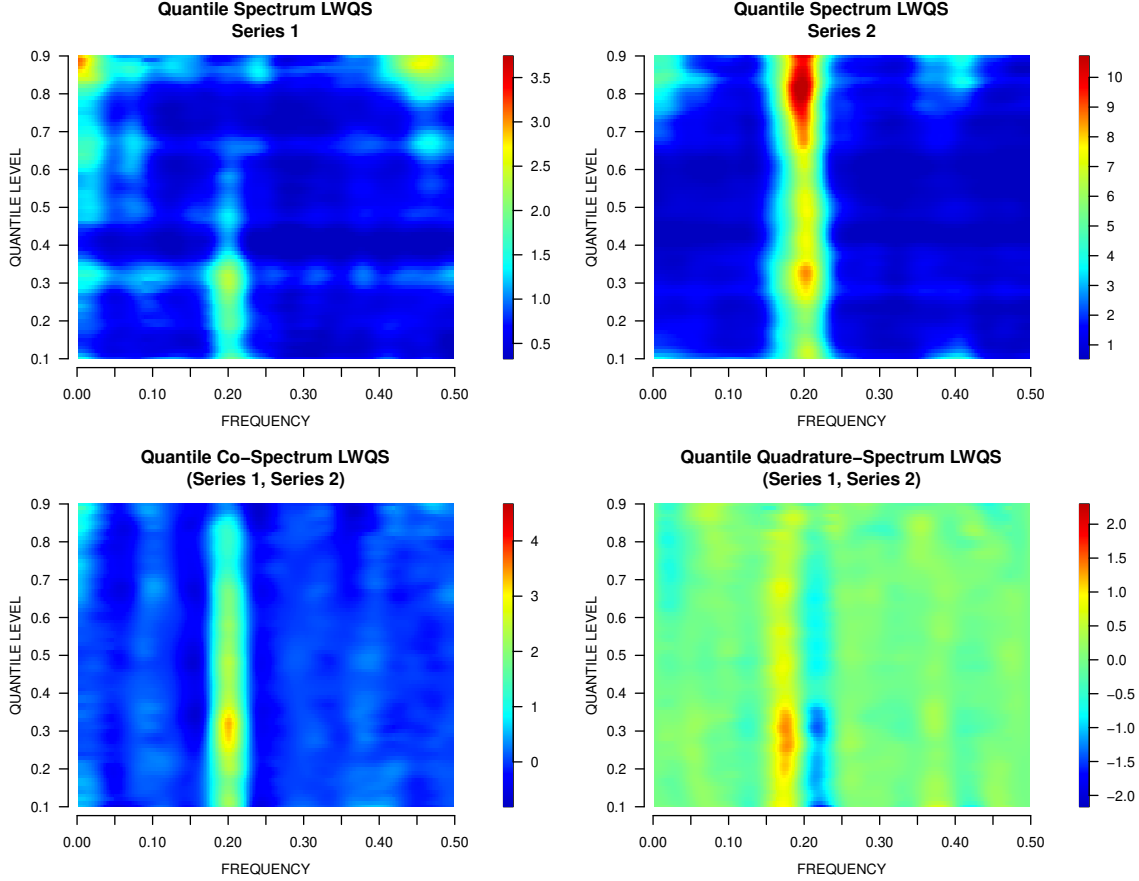


Figure 7: LWQS estimates of the quantile spectrum and cross-spectrum shown in Figure 1 from the series shown in Figure 2 using `smooth.spline` with GCV. KLD = 0.194.

as a similarity measure for time series clustering and classification (Kakizawa, Shumway, and Tanaguchi 1998). The KLD of the estimates in Figure 6 equals 0.198.

Figure 7 shows the LWQS estimates obtained by applying quantile smoothing to the LW estimates in Figure 6 using the R function `smooth.spline` with the smoothing parameter chosen by the generalized cross-validation (GCV) criterion (R Core Team 2024). The resulting KLD equals 0.194. In this case, the KLD is reduced slightly, but the effect of quantile smoothing is barely noticeable when compared to Figure 6.

A better result is shown in Figure 8. These estimates are also obtained by applying the R function `smooth.spline` to the LW estimates in Figure 6, but the smoothing parameter `spar` is

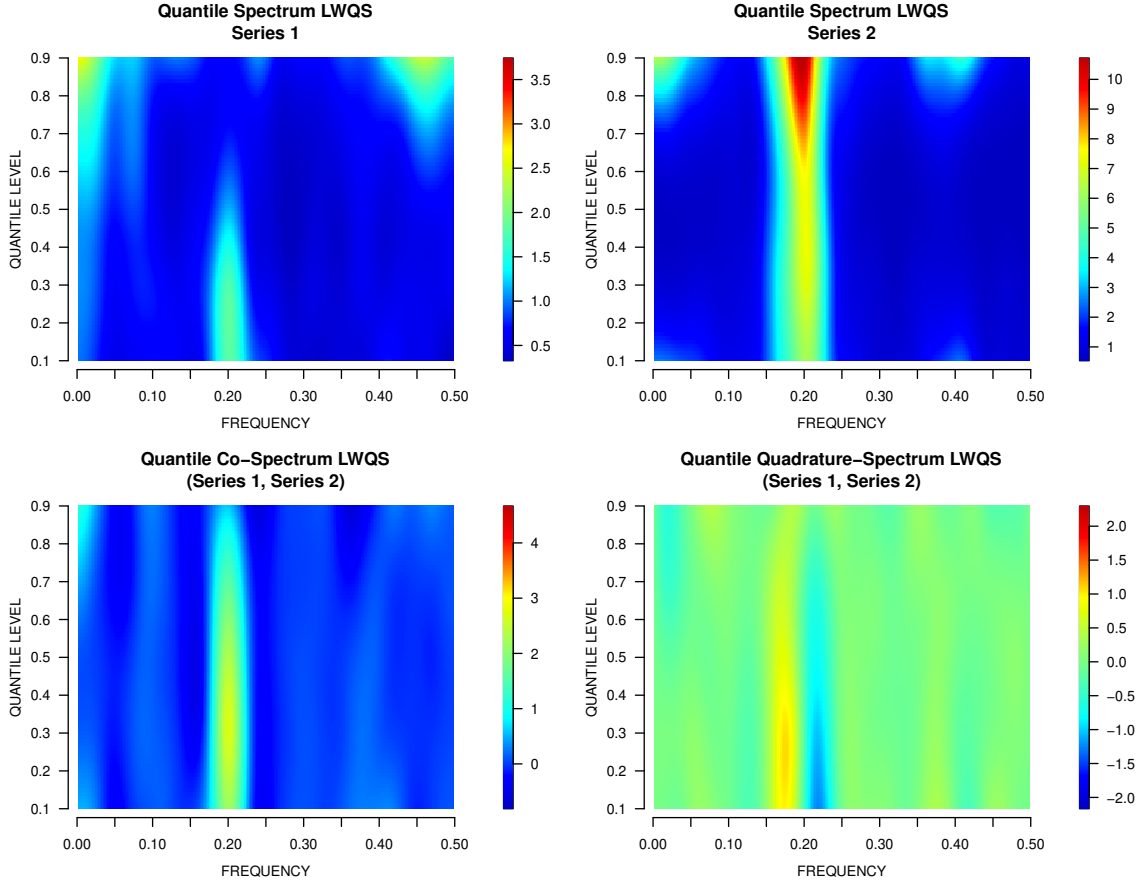


Figure 8: LWQS estimates of the quantile spectrum and cross-spectrum shown in Figure 1 for the series shown in Figure 2 using `smooth.spline` with `spar = 0.9`.  $KLD = 0.109$ .

set to 0.9 instead of being determined by GCV. The estimates in Figure 8 appear less noisy when compared to the estimates in Figures 6 and 7. The KLD is reduced significantly from 0.198 and 0.194, respectively, to 0.109.

A closer examination of the LW estimates reveals strong positive correlations across quantiles. These correlations are not handled effectively by `smooth.spline` with GCV. To take the correlations into account, we use the R function `gamm` in the ‘`mgcv`’ package (Wood 2022). Under the framework of generalized additive mixture models (Wang 1998), this function jointly estimates the smoothing splines and the parameters of a user-specified correlation structure for the random effect while retaining GCV for smoothing parameter selection.

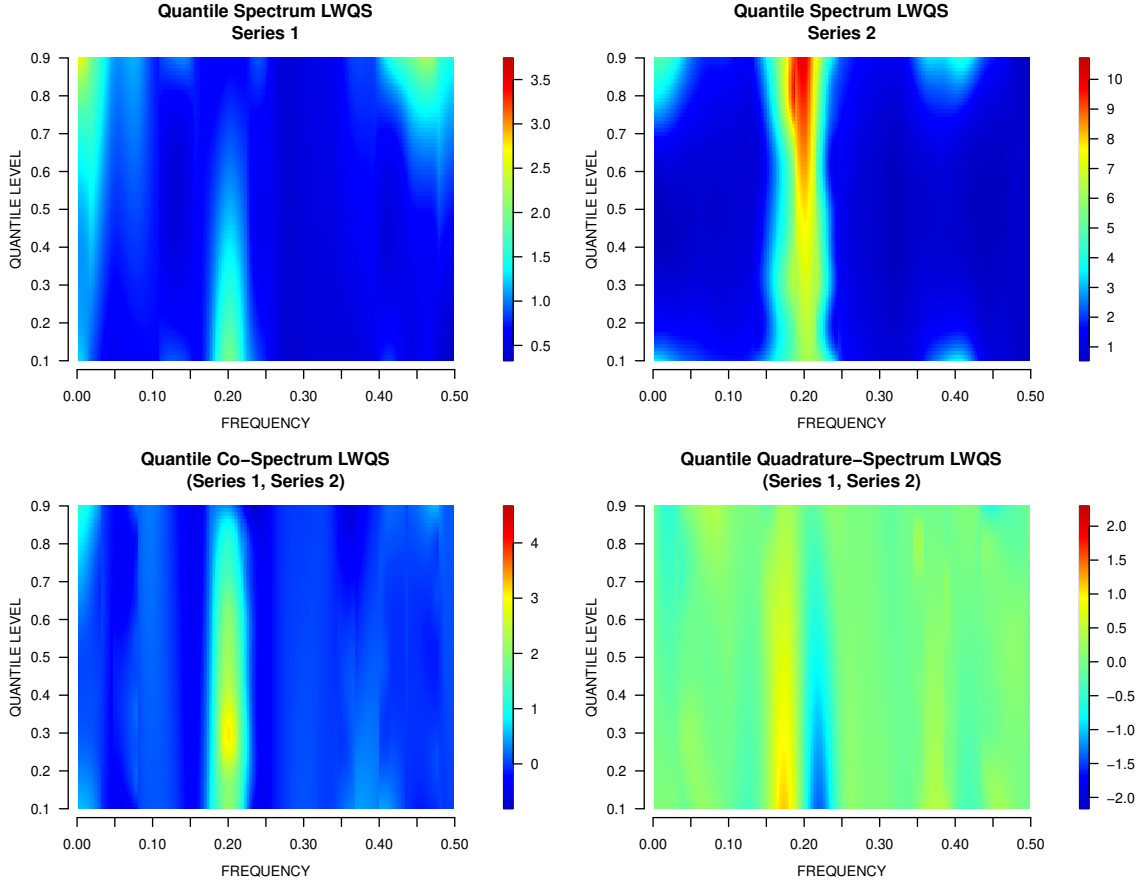


Figure 9: LWQS estimates of the quantile spectrum and cross-spectrum shown in Figure 1 from the series shown in Figure 2 using `gamm` with correlated residuals.  $KLD = 0.130$ .

Figure 9 shows the result of applying `gamm` to the LW estimates in Figure 6 assuming the correlation structure of an AR(1) process. The  $KLD$  of these estimates equals 0.130, which is a significant improvement over `smooth.spline` with GCV. This improvement is achieved at a higher computational cost: a 100-fold increase in computing time when compared to `smooth.spline`. Computation can be accelerated by parallelization for different frequencies.

Figure 10 and Table 11 provide a more comprehensive assessment of the LWQS estimator using `smooth.spline` and `gamm`. The results are based on 1000 Monte Carlo runs. As shown in Figure 10, `smooth.spline` with GCV offers a slight improvement over no quantile smoothing; a significant improvement can be made by setting `spar` manually within a range of values, with the

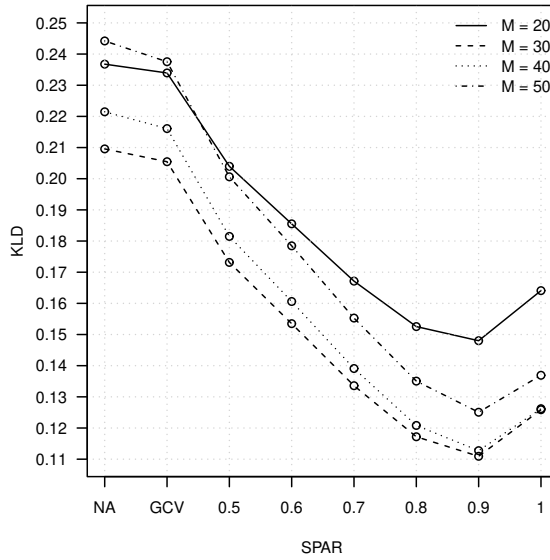


Figure 10: Mean Kullback-Leibler divergence (KLD) of the LWQS estimator for different bandwidth parameter  $M$  when quantile smoothing is performed by `smooth.spline` with different smoothing parameter `spar` (NA for no quantile smoothing). Results are based on 1000 Monte Carlo runs with quantile levels  $0.04, 0.05, \dots, 0.96$ .

Figure 11: Mean Kullback-Leibler Divergence of the LWQS Estimator

Quantile Smoothing Method	$M = 20$	$M = 30$	$M = 40$	$M = 50$
no quantile smoothing	0.237 (0.031)	0.210 (0.026)	0.221 (0.025)	0.244 (0.025)
<code>smooth.spline</code> with GCV	0.234 (0.031)	0.205 (0.026)	0.216 (0.025)	0.238 (0.025)
<code>smooth.spline</code> with <code>spar = 0.9</code>	0.148 (0.020)	0.111 (0.015)	0.113 (0.015)	0.125 (0.016)
<code>gamm</code> with correlated residuals	0.168 (0.028)	0.135 (0.023)	0.141 (0.024)	0.157 (0.025)

Results are based on 1000 Monte Carlo runs with quantile levels  $0.04, 0.05, \dots, 0.96$ . Standard error is shown in parentheses.

optimal choice being `spar = 0.9`. Furthermore, Table 11 confirms the superiority of `gamm` over `smooth.spline` for the LWQS estimator when the smoothing parameter is selected by GCV.

## 5 Concluding Remarks

In this paper, we propose a nonparametric method for estimating the quantile spectra and cross-spectra introduced through trigonometric quantile regression in Li (2012; 2014). This method is based on the quantile discrete Fourier transform (QDFT) defined by the trigonometric quantile regression and the quantile series (QSER) defined by the inverse Fourier transform of the QDFT. The autocovariance function of the QSER, or QACF, facilitates the construction of a lag-window (LW) spectral estimator for the quantile spectra and cross-spectra.

We also consider the application of a smoothing procedure to the LW estimates across quantiles in order to further improve the estimation accuracy when the underlying spectrum is smooth with respect to the quantile level variable. The quantile smoothing procedure turns out to be more effective when the observed positive correlation across quantiles is taken into account.

The nonparametric method in this paper complements the semi-parametric method investigated in Chen et al. (2021) and Jiménez-Varón et al. (2024). The latter fits a parametric autoregressive (AR) model for the QSER on a grid of quantile levels and then applies a nonparametric smoothing procedure to the AR parameters across quantiles. While the AR models in these papers are derived from the quantile periodogram, the introduction of QSER in this paper provides the possibility for a more direct approach to AR modeling: one can simply fit an AR model to the QSER directly by least squares or through the QACF by solving the Yule-Walker equations. A comprehensive treatment of this approach will be the topic of a future paper.

# References

- Brockwell, P., and Davis, R. (1991) *Time Series: Theory and Methods*, 2nd edn, section 11.6. New York: Springer.
- Baruník, J., and Kley, T. (2019) Quantile coherency: A general measure for dependence between cyclical economic variables. *Econometrics Journal*, 22, 131–152.
- Chen, T., Sun, Y., and Li, T.-H. (2021) A semiparametric estimation algorithm for the quantile spectrum with an application to earthquake classification using convolutional neural network. *Computational Statistics & Data Analysis*, 154, 107069.
- Davis, R., and Mikosch, T. (2009) The extremogram: A correlogram for extreme events. *Bernoulli*, 15, 977–1009.
- Dette, H., Hallin, M., Kley, T. and Volgushev, S. (2015) Of copulas, quantiles, ranks and spectra: an  $L_1$ -approach to spectral analysis. *Bernoulli*, 21, 781–831.
- Hagemann, A. (2013) Robust spectral analysis. arXiv:1111.1965.
- Jiménez-Varón, C., Sun, Y., and Li, T.-H. (2024) A semi-parametric estimation method for quantile coherence with an application to bivariate financial time series clustering. *Econometrics and Statistics*. <https://doi.org/10.1016/j.ecosta.2024.101111>
- Kakizawa, Y., Shumway, R., and Tanaguchi, M. (1998) Discrimination and clustering for multivariate time series. *Journal of the American Statistical Association*, 93, 328–340.
- Koenker, R. (2005) *Quantile Regression*. Cambridge, UK: Cambridge University Press.
- Li, T.-H. (2012) Quantile periodograms. *Journal of the American Statistical Association*, 107, 765–776.
- Li, T.-H. (2014) *Time Series with Mixed Spectra*. Boca Raton, FL: CRC Press.
- Li, T.-H. (2020) From zero crossings to quantile-frequency analysis of time series with an application to nondestructive evaluation. *Applied Stochastic Models for Business and Industry*, 36, 1111–1130.
- Priestley, M. (1981) *Spectral Analysis and Time Series*, p. 443. New York: Academic Press.
- R Core Team (2024) R: A language and environment for statistical computing. R Foundation for Statistical Computing, Vienna, Austria. <https://www.R-project.org/>.
- Wang, Y. (1998) Smoothing spline models with correlated random errors. *Journal of the American Statistical Association*, 93, 341–348.

Whittle, P. (1953) Estimation and information in stationary time series. *Arkiv för Matematik*, 2, 423–434.

Wood, S. (2022) Package ‘mgcv’. <https://cran.r-project.org/web/packages/mgcv/mgcv.pdf>.

Wu, W. (2007)  $M$ -estimation of linear models with dependent errors. *Annals of Statistics*, 35, 495–521.

## Appendix I: The R Functions

The following is a summary of the relevant R functions for the proposed method. These functions are available in the R package ‘qfa’ (version 3.0) which can be installed from <https://cran.r-project.org>. An installable R package `qfa_3.0.tar.gz` is also available at <https://github.com/thl2019/QFA>.

- `qdft`: a function that computes the quantile discrete Fourier transform (QDFT) of a univariate or multivariate time series at a user-specified sequence of quantile levels.
- `qser`: a function that computes the quantile series (QSER) of a univariate or multivariate time series at a user-specified sequence of quantile levels from the time series or the QDFT produced by `qdft`.
- `qacf`: a function that computes the quantile autocovariance function (QACF) of a univariate or multivariate time series at a user-specified sequence of quantile levels from the time series or the QDFT produced by `qdft`.
- `qspec.lw`: a function that computes the lag-window (LW) spectral estimate for a given bandwidth parameter from the QACF produced by `qacf`.
- `qspec.lwqs`: a function that computes the lag-window (LW) spectral estimate with quantile smoothing (QS) for a given bandwidth parameter directly from a time series or from the QACF produced by `qacf`.
- `qfa.plot`: a function that produces a quantile-frequency image plot for a real-valued quantile spectrum.
- `qdft2qser`: a function that computes the quantile series (QSER) from the QDFT produced by `qdft`.

- `qdft2qper`: a function that computes the quantile periodogram (QPER) from the QDFT produced by `qdft`.
- `qdft2qacf`: a function that computes the quantile autocovariance function (QACF) from the QDFT produced by `qdft`.
- `tqr.fit`: a low-level function that computes the trigonometric quantile regression (TQR) solution for a single frequency at a user-specified sequence of quantile levels.

## Appendix II: Additional Simulation Results

The (squared) quantile coherence spectrum for  $j \neq j'$  is defined as

$$C_{jj'}(\omega, \alpha) := \frac{|S_{jj'}(\omega, \alpha)|^2}{S_{jj}(\omega, \alpha) S_{j'j'}(\omega, \alpha)}. \quad (16)$$

Figure 12 shows the quantile coherence spectrum for the pair of time series defined by (14) and (15). By construction, a significant level of coherence is expected around frequency 0.2, but less pronounced at higher quantiles than low quantiles.

The quantile coherence spectrum can be estimated by plugging the respective estimates of quantile spectrum and cross-spectrum in (16). For the series shown in Figure 2, the LW and LWQS estimates of the quantile coherence spectrum are shown in Figure 13. They are obtained from the respective estimates of quantile spectrum and cross-spectrum shown in Figures 6–9. It is interesting to observe that the smaller KLD of LWQS with `gamm` for estimating the quantile spectrum and cross-spectrum does not yields a smaller ( $\ell_2$ ) error for estimating the quantile coherence spectrum, whereas `smooth.spline` with `spar = 0.9` still produces the best result.

Consider the ARMA process  $\mathbf{y}_t := [y_{1,t}, y_{2,t}]^T$  defined by

$$\mathbf{y}_t - \mathbf{A}_1 \mathbf{y}_{t-1} - \mathbf{A}_2 \mathbf{y}_{t-2} = \boldsymbol{\epsilon}_t + \mathbf{B} \boldsymbol{\epsilon}_{t-1}, \quad \{\boldsymbol{\epsilon}_t\} \sim \text{IID } \mathbf{N}(\mathbf{0}, \boldsymbol{\Sigma}), \quad (17)$$

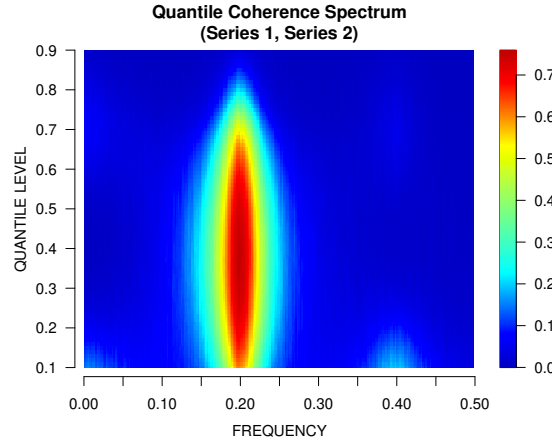


Figure 12: Simulated quantile coherence spectrum according to (14) and (15).

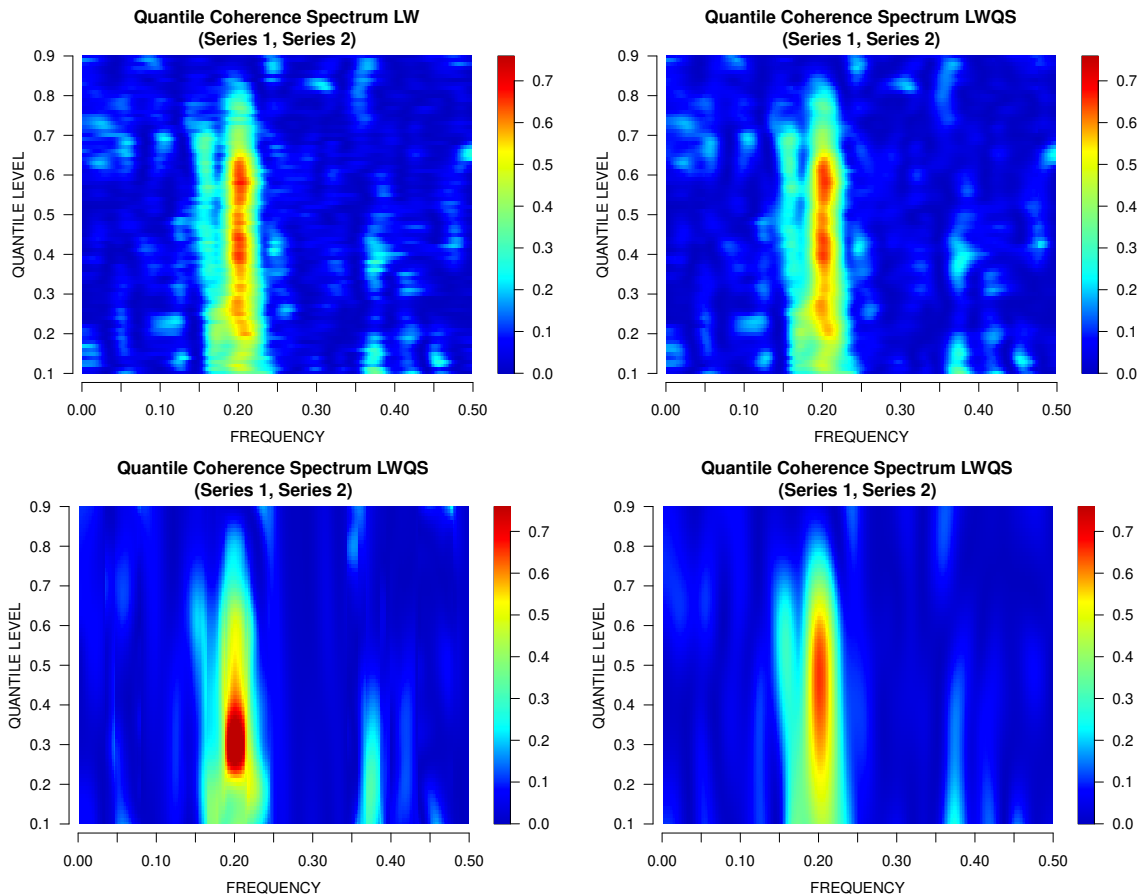


Figure 13: LW and LWQS estimates of the quantile coherence spectrum shown in Figure 12 from the series shown in Figure 2. Clockwise: (a) LW (0.078), (b) LWQS by `smooth.spline` with GCV (0.077), (c) LWQS by `smooth.spline` with `spar = 0.9` (0.065), and (d) LWQS by `gamm` (0.079). Estimation error is shown in parentheses.

where

$$\mathbf{A}_1 := \begin{bmatrix} 0.816 & 1.246 \\ 0.558 & 1.107 \end{bmatrix}, \quad \mathbf{A}_2 := \begin{bmatrix} 0.643 & 1.184 \\ 0.307 & 0.203 \end{bmatrix},$$

$$\mathbf{B} := \begin{bmatrix} 0 & 2.496 \\ 0.4 & 0 \end{bmatrix}, \quad \boldsymbol{\Sigma} := \begin{bmatrix} 0.04 & -0.02 \\ -0.02 & 0.02 \end{bmatrix}.$$

Figure 14 depicts the quantile spectrum of this process. The results for estimating this spectrum by the LWQS estimator with  $n = 512$  and various options for the bandwidth parameter and the quantile smoothing method are shown in Figure 15 and Table 16.

As in the case of the experiment in Section 4, slight improvement over LW without smoothing is achieved by `smooth.spline` with GCV, and significant improvement is achieved if the smoothing parameter takes the optimal value `spar = 1`. By assuming correlated residuals of the AR(1) type, `gamm` with correlated residuals produces more accurate estimates than `smooth.spline` with GCV at the expense of significantly higher computational burden.

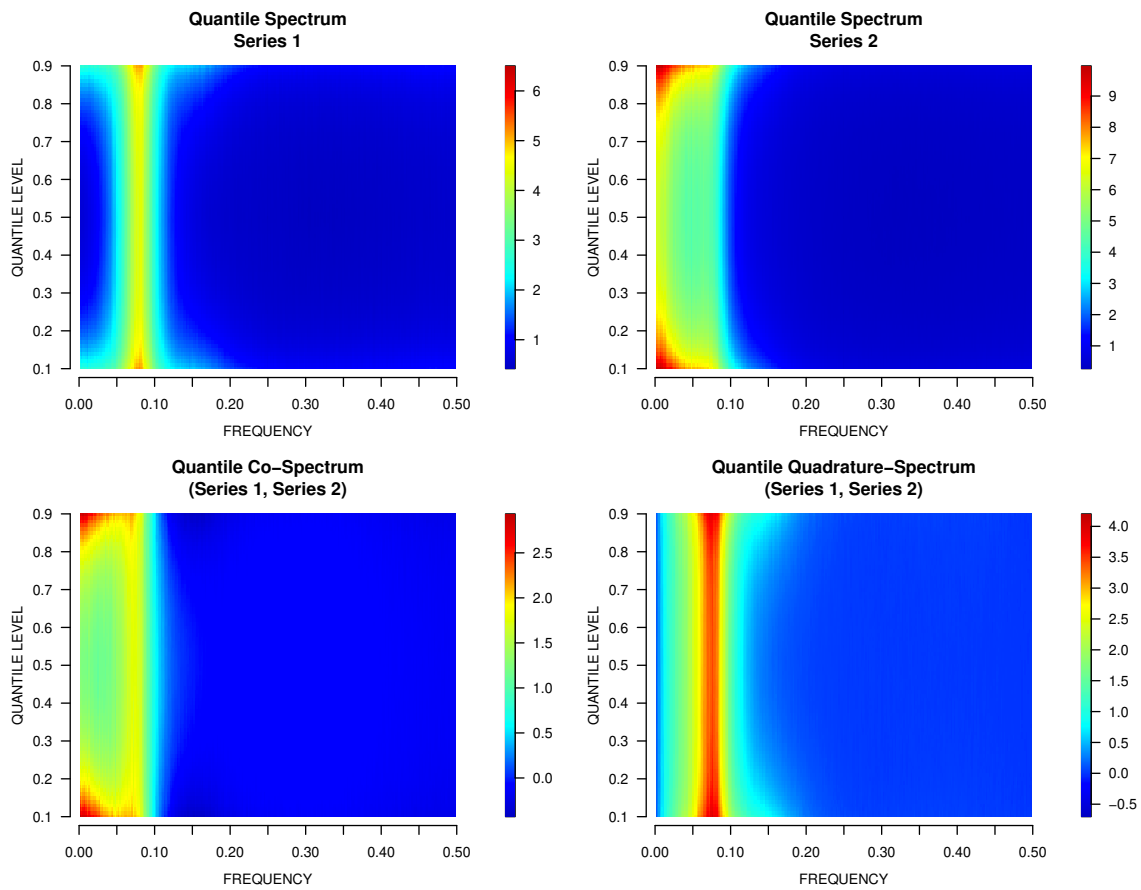


Figure 14: Quantile spectrum and cross-spectrum of the ARMA process (17).

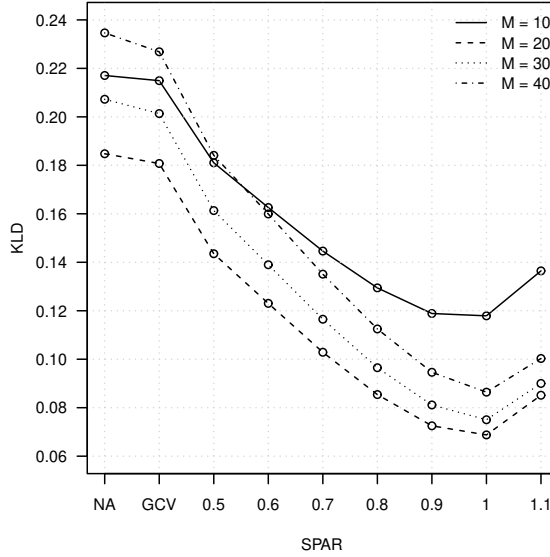


Figure 15: Mean Kullback-Leibler divergence (KLD) of the LWQS estimator for the ARMA process (17) with different bandwidth parameter  $M$  when quantile smoothing is performed by `smooth.spline` with different smoothing parameter `spar` (NA for no quantile smoothing). Results are based on 1000 Monte Carlo runs with quantile levels  $0.10, 0.11, \dots, 0.90$ .

Figure 16: Mean KLD of the LWQS Estimator for the AMAR Process (17)

Quantile Smoothing Method	$M = 10$	$M = 20$	$M = 30$	$M = 40$
no quantile smoothing	0.217 (0.045)	0.185 (0.034)	0.207 (0.033)	0.235 (0.033)
<code>smooth.spline</code> with GCV	0.215 (0.045)	0.181 (0.033)	0.201 (0.033)	0.227 (0.033)
<code>smooth.spline</code> with <code>spar = 1</code>	0.118 (0.032)	0.069 (0.022)	0.075 (0.023)	0.086 (0.024)
<code>gamm</code> with correlated residuals	0.150 (0.042)	0.105 (0.029)	0.117 (0.029)	0.133 (0.028)

Results are based on 1000 Monte Carlo runs with quantile levels  $0.10, 0.11, \dots, 0.90$ . Standard error is shown in parentheses.